An element-free Galerkin (EFG) method for numerical solution of the coupled Schrödinger-KdV equations*

Liu Yong-Qing(刘永庆)[a], Cheng Rong-Jun(程荣军)[b], and Ge Hong-Xia(葛红霞)[c]†

[a] Faculty of Science, Ningbo University, Ningbo 315211, China
[b] Ningbo Institute of Technology, Zhejiang University, Ningbo 315100, China
[c] Faculty of Maritime and Transportation, Ningbo University, Ningbo 315211, China

(Received 19 October 2012; revised manuscript received 7 April 2013)

The present paper deals with the numerical solution of the coupled Schrödinger-KdV equations using the element-free Galerkin (EFG) method which is based on the moving least-square approximation. Instead of traditional mesh oriented methods such as the finite difference method (FDM) and the finite element method (FEM), this method needs only scattered nodes in the domain. For this scheme, a variational method is used to obtain discrete equations and the essential boundary conditions are enforced by the penalty method. In numerical experiments, the results are presented and compared with the findings of the finite element method, the radial basis functions method, and an analytical solution to confirm the good accuracy of the presented scheme.

Keywords: element-free Galerkin (EFG) method, meshless method, the coupled Schrödinger-KdV equations

PACS: 02.60.Lj, 03.65.Ge **DOI:** 10.1088/1674-1056/22/10/100204

1. Introduction

There has been a surge of interest in the family of nonlinear Schrödinger equations because of their many applications to various kinds of physical phenomena. The coupled Schrödinger-KdV equations[1]

$$\mathrm{i}\epsilon E_t + \frac{3}{2}E_{xx} - \frac{1}{2}NE = 0, \tag{1}$$

$$N_t + \frac{1}{2}N_{xxx} + \frac{1}{2}(N^2 + |E|^2)_x = 0, \tag{2}$$

have been widely used to model the nonlinear dynamics of one-dimensional Langmuir and ion-acoustic waves in a system of coordinates moving at the ion-acoustic speed. In Eqs. (1) and (2), N is a real function describing low-frequency density perturbation and E is a complex function describing the electric field of Langmuir oscillations. $\epsilon > 0$ is a constant.

This problem has been the subject of research for many years and has motivated a series of work in physics and mathematics. The solution of Schrödinger equations has been studied by a number of authors.[2–8] The stability properties of such solutions for external perturbations has also been presented.[1,8] Recently, various techniques, such as variational iteration method[9] and decomposition method,[10] have been widely used to solve this problem. To obtain a numerical solution of the coupled Schrödinger–KdV equations, Appert and Vaclavik used the finite difference Crank–Nicolson (CN) scheme,[1] Bai and Zhang used the finite element method,[11] and Golbabai and Safdari-Vaighani used the radial basis function method.[12]

In the last decade, the meshless method, which is a new and efficient numerical simulation technique, has gained importance for getting the numerical solution of the various types of partial differential equations. Many meshless methods have been developed, such as the radial basis functions (RBF) method. The element-free Galerkin (EFG) method, a meshless method, is greatly developed and widely used in various fields.[13–17]

In this paper, we investigate a different approach to find the solution of the coupled Schrödinger–KdV equations. The EFG method is used to obtain the numerical solution of Eqs. (1) and (2). In this method, the functions over the solution domain need only a set of nodes and it does not require element connectivity. The variational method is used to obtain the corresponding discrete equations and the essential boundary conditions are enforced by the penalty method. To test the efficiency of this scheme, we compare the estimated solution of our method by exact solution and other methods.

The remainder of the paper is organized as follows. In Section 2, we introduce the moving least-square (MLS) approximation used in the EFG method. In Section 3, the EFG method is implemented for including discrete equations of the problem. Numerical experiments are presented in Section 4. We end this paper in Section 5.

*Project supported by the National Natural Science Foundation of China (Grant Nos. 11072117 and 61074142), the Natural Science Foundation of Zhejiang Province, China (Grant No. Y6110007), Scientific Research Fund of Zhejiang Provincial Education Department, China (Grant No. Z201119278), the Natural Science Foundation of Ningbo City (Grant Nos. 2012A610152 and 2012A610038), the Disciplinary Project of Ningbo City, China (Grant No. SZXL1067), and K. C. Wong Magna Fund in Ningbo University.

†Corresponding author. E-mail: gehongxia@nbu.edu.cn

© 2013 Chinese Physical Society and IOP Publishing Ltd

2. Moving least-squares (MLS) approximation

In this approximation, Lancaster and Salkauskas[18] defined a local approximation by

$$u^h(\boldsymbol{x},\overline{\boldsymbol{x}}) = \sum_{k=1}^{m} p_k(\boldsymbol{x})a_k(\overline{\boldsymbol{x}}) \equiv \boldsymbol{P}^{\mathrm{T}}(\boldsymbol{x})\boldsymbol{a}(\overline{\boldsymbol{x}}), \tag{3}$$

where m is the number of terms in the basis, $p_k(\boldsymbol{x})$ are monomial basis functions, $a_k(\overline{\boldsymbol{x}})$ are unknown coefficients, which are functions of the spatial coordinates $\boldsymbol{x}$. The $\boldsymbol{P}^{\mathrm{T}}(\boldsymbol{x})$ is vector composed of $p_k(\boldsymbol{x})$, and $\boldsymbol{a}(\overline{\boldsymbol{x}})$ is also the vector forms of $a_k(\overline{\boldsymbol{x}})$.

To determine the unknown coefficients $\boldsymbol{a}(\overline{\boldsymbol{x}})$, we minimize the weighted discrete L_2 norm given by

$$\boldsymbol{J} = \sum_{i=1}^{n} w(\boldsymbol{x}-\boldsymbol{x}_i)[\boldsymbol{P}^{\mathrm{T}}(\boldsymbol{x}_i)\boldsymbol{a}(\boldsymbol{x}) - u(\boldsymbol{x}_i)]^2, \tag{4}$$

where $w(\boldsymbol{x}-\boldsymbol{x}_i)$ is a weight function with compact support, $\boldsymbol{x}_i$ and n are respectively the nodes and the number of nodes in the compacted supported domain of $\boldsymbol{x}$.

Then by minimizing $\boldsymbol{J}$ in Eq. (4), we have

$$\frac{\partial \boldsymbol{J}}{\partial \boldsymbol{a}} = \boldsymbol{A}(\boldsymbol{x})\boldsymbol{a}(\boldsymbol{x}) - \boldsymbol{B}(\boldsymbol{x})\boldsymbol{U} = \boldsymbol{0}, \tag{5}$$

$$\boldsymbol{a}(\boldsymbol{x}) = \boldsymbol{A}^{-1}(\boldsymbol{x})\boldsymbol{B}(\boldsymbol{x})\boldsymbol{U}, \tag{6}$$

where

$$\boldsymbol{A}(\boldsymbol{x}) = \sum_{i=1}^{N} w(\boldsymbol{x}-\boldsymbol{x}_i)\boldsymbol{P}(\boldsymbol{x}_i)\boldsymbol{P}^{\mathrm{T}}(\boldsymbol{x}_i), \tag{7}$$

$$\boldsymbol{B}(\boldsymbol{x}) = [w(\boldsymbol{x}-\boldsymbol{x}_1)\boldsymbol{P}(\boldsymbol{x}_1), w(\boldsymbol{x}-\boldsymbol{x}_2)\boldsymbol{P}(\boldsymbol{x}_2), \ldots, w(\boldsymbol{x}-\boldsymbol{x}_N)\boldsymbol{P}(\boldsymbol{x}_N)], \tag{8}$$

$$\boldsymbol{U} = [u_1, u_2, \ldots, u_N]^{\mathrm{T}}. \tag{9}$$

Now, the approximate function of $u(\boldsymbol{x})$ can be expressed as

$$u(\boldsymbol{x}) \approx u^h(\boldsymbol{x}) = \sum_{k=1}^{m} p_k(\boldsymbol{x})a_k(\boldsymbol{x}) = \sum_{i=1}^{N} \phi_i u_i = \boldsymbol{\Phi}\boldsymbol{U}, \tag{10}$$

where $\boldsymbol{\Phi}$ is a matrix of shape function, defined as

$$\boldsymbol{\Phi} = [\phi_1(\boldsymbol{x}), \phi_2(\boldsymbol{x}), \ldots, \phi_N(\boldsymbol{x})] = \boldsymbol{P}^{\mathrm{T}}(\boldsymbol{x})\boldsymbol{A}^{-1}(\boldsymbol{x})\boldsymbol{B}(\boldsymbol{x}). \tag{11}$$

The derivative of the unknown $u(\boldsymbol{x})$ is approximated by

$$\frac{\partial^q}{\partial x^q}u^h(\boldsymbol{x}) = \sum_{i=1}^{N}\left[\frac{\partial^q}{\partial x^q}\phi_i(\boldsymbol{x})\right]u_i. \tag{12}$$

The weight function plays a very important role in the MLS approximtion, so the selection of an appropriate weight function is essential. In this paper, we use the cubic spline weight function.

$$w(\boldsymbol{x}-\boldsymbol{x}_i) = w(r) = \begin{cases} \dfrac{2}{3} - 4r^2 + 4r^3, & r \le \dfrac{1}{2}, \\ \dfrac{4}{3} - 4r + 4r^2 - \dfrac{4}{3}r^3, & \dfrac{1}{2} < r \le 1, \\ 0, & r > 1 \end{cases} \tag{13}$$

with

$$r = \frac{d_i}{d_{m_i}}, \quad d_i = \|\boldsymbol{x}-\boldsymbol{x}_i\|, \quad d_{m_i} = d_{\mathrm{scale}}c_i,$$

where d_{scale} is a scaling parameter, the distance c_i is chosen so that the matrix $\boldsymbol{A}(\boldsymbol{x})$ is not singular.

3. Numerical scheme

Let us consider the coupled time-dependent Schrödinger-KdV equations with the initial and boundary conditions given by

$$E(x,0) = f(x), \quad N(x,0) = g(x), \quad a \le x \le b, \tag{14}$$

$$E(a,t) = E_1(t), \quad E(b,t) = E_2(t), \quad N(a,t) = N_1(t), \quad N(b,t) = N_2(t), \quad 0 \le t \le T. \tag{15}$$

To establish the numerical approximation scheme, we consider B points in $[a,b]$ and h is the spatial step size. The grid points in the time interval $[0,T]$ are labeled as $t_j = n\Delta t, n = 0,1,2,3,\ldots$, where Δt is the time interval. We use a weak form of the equations and employ the penalty function method to deal with the boundary conditions. By taking variation, the weak forms of Eqs. (1) and (2) are respectively

$$\int_\Gamma \delta E\,\mathrm{i}\epsilon\left(E_t + \frac{3}{2}E_{xx} - \frac{1}{2}NE\right)\mathrm{d}\Gamma + \alpha\delta E(E-E_0)|_{x=a,x=b} = 0, \tag{16}$$

$$\int_\Gamma \delta N\left(N_t + \frac{1}{2}N_{xxx} + \frac{1}{2}(N^2+|E|^2)_x\right)\mathrm{d}\Gamma + \alpha\delta N(N-N_0)|_{x=a,x=b} = 0, \tag{17}$$

where Γ refers to the domain of x. In the boundaries, the values of E is E_0, and the values of N is N_0. α is a penalty parameter which usually equals $10^5 \sim 10^{12}$.

Equations (16) and (17) can also be written as

$$\int_\Gamma \delta E\,\mathrm{i}\epsilon E_t\,\mathrm{d}\Gamma - \frac{3}{2}\int_\Gamma \delta E_x E_x z\,\mathrm{d}\Gamma - \frac{1}{2}\int_\Gamma \delta E N E\,\mathrm{d}\Gamma + \alpha\delta E(E-E_0)|_{x=a,x=b} = 0, \tag{18}$$

$$\int_\Gamma \delta N N_t\,\mathrm{d}\Gamma - \frac{1}{2}\int_\Gamma \delta N_x N_{xx}\,\mathrm{d}\Gamma - \frac{1}{2}\int_\Gamma \delta N_x(N^2+|E|^2)\,\mathrm{d}\Gamma + \alpha\delta N(N-N_0)|_{x=a,x=b} = 0. \tag{19}$$

From Eqs. (10) and (12), we can obtain the approximations of E, E_t, E_x, N, N_t, and N_x

$$E = \sum_{i=1}^{B}\phi_i(x)u_i(t) = \boldsymbol{\Phi}(x)\boldsymbol{U}(t),$$

$$N = \sum_{i=1}^{B}\phi_i(x)m_i(t) = \boldsymbol{\Phi}(x)\boldsymbol{M}(t), \tag{20}$$

$$E_x = \sum_{i=1}^{B} \frac{\partial \phi_i(x)}{\partial x} u_i(t) = \Phi_x(x)\boldsymbol{U}(t),$$
$$N_x = \sum_{i=1}^{B} \frac{\partial \phi_i(x)}{\partial x} m_i(t) = \Phi_x(x)\boldsymbol{M}(t), \quad (21)$$
$$E_t = \sum_{i=1}^{B} \phi_i(x) \frac{\partial u_i(t)}{\partial t} = \Phi(x)\boldsymbol{U}(t),$$
$$N_t = \sum_{i=1}^{B} \phi_i(x) \frac{\partial m_i(t)}{\partial t} = \Phi(x)\boldsymbol{M}(t), \quad (22)$$

where

$$\boldsymbol{U}(t) = [u_1(t),\ u_2(t),\ u_3(t),\ \ldots, u_B(t)]^{\mathrm{T}}, \quad (23)$$
$$\boldsymbol{M}(t) = [m_1(t),\ m_2(t),\ m_3(t),\ \ldots, m_B(t)]^{\mathrm{T}}, \quad (24)$$
$$\Phi(x) = [\phi_1(x),\ \phi_2(x),\ \phi_3(x), \ldots, \phi_B(x)], \quad (25)$$
$$\Phi_x(x) = [\phi_{1,x}(x), \phi_{2,x}(x), \phi_{3,x}(x), \ldots, \phi_{B,x}(x)]. \quad (26)$$

Substituting Eqs. (20)–(22) into Eqs. (18) and (19) yields

$$\delta \boldsymbol{U}^{\mathrm{T}} \mathrm{i}\epsilon \int_\Gamma \Phi^{\mathrm{T}} \Phi \mathrm{d}\Gamma \dot{\boldsymbol{U}} - \frac{3}{2}\delta \boldsymbol{U}^{\mathrm{T}} \int_\Gamma \Phi_x^{\mathrm{T}} \Phi_x \mathrm{d}\Gamma \boldsymbol{U} - \frac{1}{2}\delta \boldsymbol{U}^{\mathrm{T}} \int_\Gamma \Phi^{\mathrm{T}} NE \mathrm{d}\Gamma + \alpha \delta \boldsymbol{U}^{\mathrm{T}} \Phi^{\mathrm{T}} (\Phi \boldsymbol{U} - E_0)|_{x=a,x=b} = 0, \quad (27)$$

$$\delta \boldsymbol{M}^{\mathrm{T}} \int_\Gamma \Phi^{\mathrm{T}} \Phi \mathrm{d}\Gamma \dot{\boldsymbol{M}} - \frac{1}{2}\delta \boldsymbol{M}^{\mathrm{T}} \int_\Gamma \Phi_x^{\mathrm{T}} \Phi_{xx} \mathrm{d}\Gamma \boldsymbol{M} - \frac{1}{2}\delta \boldsymbol{M}^{\mathrm{T}} \int_\Gamma \Phi_x^{\mathrm{T}} (N^2 + |E|^2) \mathrm{d}\Gamma + \alpha \delta \boldsymbol{M}^{\mathrm{T}} \Phi^{\mathrm{T}} (\Phi \boldsymbol{M} - N_0)|_{x=a,x=b} = 0. \quad (28)$$

According to the arbitrariness of $\delta \boldsymbol{U}^{\mathrm{T}}$ and $\delta \boldsymbol{M}^{\mathrm{T}}$, equations (27) and (28) become

$$\mathrm{i}\epsilon \boldsymbol{C}\dot{\boldsymbol{U}} + \boldsymbol{Ke}\boldsymbol{U} - \frac{1}{2}\int_\Gamma \Phi^{\mathrm{T}} NE \mathrm{d}\Gamma + \boldsymbol{Fe} = 0, \quad (29)$$

$$\boldsymbol{C}\dot{\boldsymbol{M}} + \boldsymbol{Kn}\boldsymbol{M} - \frac{1}{2}\int_\Gamma \Phi_x^{\mathrm{T}} (N^2 + |E|^2) \mathrm{d}\Gamma + \boldsymbol{Fn} = 0, \quad (30)$$

where $\boldsymbol{C}$, $\boldsymbol{Ke}$, and $\boldsymbol{Kn}$ are $B \times B$ matrices, $\boldsymbol{Fe}$ and $\boldsymbol{Fn}$ are $B \times 1$ matrices

$$\boldsymbol{C} = \int_\Gamma \Phi^{\mathrm{T}} \Phi \mathrm{d}\Gamma, \quad (31)$$
$$\boldsymbol{Fe} = -\alpha(\Phi^{\mathrm{T}} E_0|_{x=a} + \Phi^{\mathrm{T}} E_0|_{x=b}), \quad (32)$$
$$\boldsymbol{Fn} = -\alpha(\Phi^{\mathrm{T}} N_0|_{x=a} + \Phi^{\mathrm{T}} N_0|_{x=b}), \quad (33)$$
$$\boldsymbol{Ke} = -\frac{3}{2}\int_\Gamma \Phi_x^{\mathrm{T}} \Phi_x \mathrm{d}\Gamma + \alpha(\Phi^{\mathrm{T}} \Phi|_{x=a} + \Phi^{\mathrm{T}} \Phi|_{x=b}), \quad (34)$$
$$\boldsymbol{Kn} = -\frac{1}{2}\int_\Gamma \Phi_x^{\mathrm{T}} \Phi_{xx} \mathrm{d}\Gamma + \alpha(\Phi^{\mathrm{T}} \Phi|_{x=a} + \Phi^{\mathrm{T}} \Phi|_{x=b}). \quad (35)$$

We use the forward finite difference approximation for the time derivative. The following scheme from Eqs. (29) and (30) can be obtained

$$\mathrm{i}\epsilon \boldsymbol{C}\frac{\boldsymbol{U}^{n+1} - \boldsymbol{U}^n}{\Delta t} + \boldsymbol{Ke}\boldsymbol{U}^{n+1/2} - \frac{1}{2}\int_\Gamma \Phi^{\mathrm{T}} (NE)^{n+1/2} \mathrm{d}\Gamma + \boldsymbol{Fe}^{n+1/2} = 0, \quad (36)$$

$$\boldsymbol{C}\frac{\boldsymbol{M}^{n+1} - \boldsymbol{M}^n}{\Delta t} + \boldsymbol{Kn}\boldsymbol{M}^{n+1/2} - \frac{1}{2}\int_\Gamma \Phi_x^{\mathrm{T}} (N^2 + E\overline{E})^{n+1/2} \mathrm{d}\Gamma + \boldsymbol{Fn}^{n+1/2} = 0, \quad (37)$$

where

$$t^{n+1} = (n+1)\Delta t, \ \ E^{n+1} = E(x, t^{n+1}),$$
$$N^{n+1} = N(x, t^{n+1}), \ \ \boldsymbol{U}^{n+1/2} = \frac{\boldsymbol{U}^n + \boldsymbol{U}^{n+1}}{2}.$$

Other terms of notation are similar to E^{n+1} and $\boldsymbol{U}^{n+1/2}$. $\overline{E}$ is the complex conjugate of E.

The nonlinear terms in Eqs. (36) and (37) are linearized by using the following term[19]

$$(NE)^{n+1} = N^{n+1}E^n + N^n E^{n+1} - N^n E^n,$$
$$(N^2)^{n+1} = N^{n+1}N^n + N^n N^{n+1} - N^n N^n,$$
$$(E\overline{E})^{n+1} = E^{n+1}\overline{E}^n + E^n \overline{E}^{n+1} - E^n \overline{E}^n.$$

Now, our equations can be written as

$$\mathrm{i}\epsilon \boldsymbol{C}\frac{\boldsymbol{U}^{n+1} - \boldsymbol{U}^n}{\Delta t} + \boldsymbol{Ke}\boldsymbol{U}^{n+1/2} - \frac{1}{2}\int_\Gamma \Phi^{\mathrm{T}} \frac{N^{n+1}E^n + N^n E^{n+1}}{2} \mathrm{d}\Gamma + \boldsymbol{Fe}^{n+1/2} = 0, \quad (38)$$

$$\boldsymbol{C}\frac{\boldsymbol{M}^{n+1} - \boldsymbol{M}^n}{\Delta t} + \boldsymbol{Kn}\boldsymbol{M}^{n+1/2} - \frac{1}{2}\int_\Gamma \Phi_x^{\mathrm{T}} \frac{2N^{n+1}N^n + E^{n+1}\overline{E}^n + E^n \overline{E}^{n+1}}{2} \mathrm{d}\Gamma + \boldsymbol{Fn}^{n+1/2} = 0. \quad (39)$$

Assume that $U^n = U_r^n + \mathrm{i}U_i^n$ and $Fe^{n+1/2} = Fe_r^{n+1/2} + \mathrm{i}Fe_i^{n+1/2}$, where U_r^n, $Fe_r^{n+1/2}$ respectively denote the real part of U^n and $Fe^{n+1/2}$; U_i^n, $Fe_i^{n+1/2}$ respectively denote the imaginary part of U^n and $Fe^{n+1/2}$. By using this notation, equating the real part and imaginary part of the right and left sides of Eq. (38), Eqs. (38) and (39) can be written as

$$\boldsymbol{A}\boldsymbol{U}_r^{n+1} + \boldsymbol{E}\boldsymbol{U}_i^{n+1} + \boldsymbol{B}_r \boldsymbol{M}^{n+1} = \boldsymbol{D}\boldsymbol{U}_r^n + \boldsymbol{E}\boldsymbol{U}_i^n + \boldsymbol{Fe}_r^{n+1/2}, \quad (40)$$

$$-\boldsymbol{E}\boldsymbol{U}_r^{n+1} + \boldsymbol{A}\boldsymbol{U}_i^{n+1} + \boldsymbol{B}_i \boldsymbol{M}^{n+1} = -\boldsymbol{E}\boldsymbol{U}_r^n + \boldsymbol{D}\boldsymbol{U}_i^n + \boldsymbol{Fe}_i^{n+1/2}, \quad (41)$$

$$\boldsymbol{Q}_r \boldsymbol{U}_r^{n+1} + \boldsymbol{Q}_i \boldsymbol{U}_i^{n+1} + \boldsymbol{P}\boldsymbol{M}^{n+1} = \boldsymbol{S}\boldsymbol{M}^n - \boldsymbol{Fn}^{n+1/2}, \quad (42)$$

where

$$\boldsymbol{E} = \frac{\epsilon \boldsymbol{C}}{\triangle t}, \ \ \boldsymbol{D} = \frac{\boldsymbol{Ke}}{2}, \quad (43)$$

$$\boldsymbol{S} = \frac{\boldsymbol{C}}{\triangle t} - \frac{\boldsymbol{Ke}}{2}, \ \ \boldsymbol{B}_r = \frac{1}{4}\int_\Gamma \Phi^{\mathrm{T}} \Phi \boldsymbol{U}_r^n \Phi \mathrm{d}\Gamma, \quad (44)$$

$$\boldsymbol{B}_i = \frac{1}{4}\int_\Gamma \Phi^{\mathrm{T}} \Phi \boldsymbol{U}_i^n \Phi \mathrm{d}\Gamma,$$

$$\boldsymbol{Q}_r = -\frac{1}{2}\int_\Gamma \Phi_x^{\mathrm{T}} \Phi \boldsymbol{U}_r^n \Phi \mathrm{d}\Gamma, \quad (45)$$

$$\boldsymbol{Q}_i = -\frac{1}{2}\int_\Gamma \Phi_x^{\mathrm{T}}\Phi \boldsymbol{U}_i^n \Phi \mathrm{d}\Gamma,$$

$$\boldsymbol{A} = \frac{1}{4}\int_\Gamma \Phi^{\mathrm{T}}\Phi \boldsymbol{M}^n \Phi \mathrm{d}\Gamma - \frac{\boldsymbol{Ke}}{2}, \tag{46}$$

$$\boldsymbol{P} = \frac{\boldsymbol{C}}{\triangle t} + \frac{\boldsymbol{Kn}}{2} - \frac{1}{2}\int_\Gamma \Phi_x^{\mathrm{T}}\Phi \boldsymbol{M}^n \Phi \mathrm{d}\Gamma. \tag{47}$$

Now equations (40)–(42) can be rewritten in the following form

$$\begin{pmatrix} \boldsymbol{A} & \boldsymbol{E} & \boldsymbol{B}_r \\ -\boldsymbol{E} & \boldsymbol{A} & \boldsymbol{B}_i \\ \boldsymbol{Q}_r & \boldsymbol{Q}_i & \boldsymbol{P} \end{pmatrix} \begin{pmatrix} \boldsymbol{U}_r^{n+1} \\ \boldsymbol{U}_i^{n+1} \\ \boldsymbol{M}^{n+1} \end{pmatrix} = \begin{pmatrix} \boldsymbol{D} & \boldsymbol{E} & \boldsymbol{0} \\ -\boldsymbol{E} & \boldsymbol{D} & \boldsymbol{0} \\ \boldsymbol{0} & \boldsymbol{0} & \boldsymbol{S} \end{pmatrix} \begin{pmatrix} \boldsymbol{U}_r^{n} \\ \boldsymbol{U}_i^{n} \\ \boldsymbol{M}^{n} \end{pmatrix} + \begin{pmatrix} \boldsymbol{Fe}_r^{n+1/2} \\ \boldsymbol{Fe}_i^{n+1/2} \\ -\boldsymbol{Fn}^{n+1/2} \end{pmatrix}. \tag{48}$$

Equations (48) are the discrete expression of the coupled Schrödinger-KdV equations. Through Eqs. (48), we can get any moment parameters $\boldsymbol{U}^{n+1}$ and $\boldsymbol{M}^{n+1}$, then by substituting $\boldsymbol{U}^{n+1}$ and $\boldsymbol{M}^{n+1}$ into Eqs. (20) and (21), the approximation solutions of the coupled Schrödinger-KdV equations are known.

4. Numerical example

In this section, the application of the EFG method to the coupled Schrödinger-KdV equations is demonstrated by examples for which exact solutions are known. In our examples, a regular arrangement of nodes is used, and a cell structure is used to set the quadrature cells equal to the intervals between the nodes. In each integration cell, a 4-Gauss quadrature scheme is used to evaluate the stiffness matrix. For comparison of this method with other methods, we compute the error norms L_2, L_∞ to illustrate the accuracy of the method

$$L_2 = \|u-u^h\|_2 = \sqrt{h\sum_{j=1}^{B}(u(x_j,t)-u^h(x_j,t))^2}, \tag{49}$$

$$L_\infty = \|u-u^h\|_\infty = \max_{1\le j\le B}|u(x_j,t)-u^h(x_j,t)|, \tag{50}$$

where h is the spatial step size, B is the number of points.

The exact solution to Eqs. (1) and (2) was derived[20] as

$$N(x,t) = -\frac{9}{5}\beta\frac{1}{\cosh^2\xi}, \tag{51}$$

$$E(x,t) = -\frac{6}{5}\sqrt{3}\beta\frac{\tanh\xi}{\cosh\xi} \times \exp\left[\mathrm{i}\beta\left[\left(\frac{3}{20\epsilon}-\frac{\epsilon\beta}{6}\right)t-\frac{\epsilon x}{3}\right]\right], \tag{52}$$

where $\xi = \sqrt{\beta/10}(x-\beta t)$ and β is an arbitrary positive constant. We take the value of the exact solution at $t=0$ as our initial conditions

$$N(x,0) = -\frac{9}{5}\beta\frac{1}{\cosh^2\xi}, \tag{53}$$

$$E(x,0) = -\frac{6}{5}\sqrt{3}\beta\frac{\tanh\xi}{\cosh\xi} \times \mathrm{e}^{\mathrm{i}\beta(-\epsilon x/3)}, \tag{54}$$

where $\xi = \sqrt{\beta/10}x$.

We solve the problem by the present method with penalty factor $\alpha = 1\times10^{10}$, $\epsilon = 1$, $\beta = 0.45$, scaling parameter $d_{\mathrm{scale}} = 2.1$, the time step length $\Delta t = 10^{-4}$, spatial interval $[-30, 30]$, and the spatial step size $h = 0.25$. The weight function is chosen to be a cubic spline function and the bases are chosen to be linear.

Figures 1 and 2 show exact solution and estimate solution of $|E|$ (modulus of $E(x,t)$), E_{r} (real part of $E(x,t)$), E_{i} (imaginary part of $E(x,t)$), and N at different values of time. It can be found that slight increases of the error obtained as we increase the value of time. The comparative results are shown in Tables 1–3 and the comparative of the error norms are reported in Tables 4 and 5. These tables display that the results obtained by EFG method are much better than those gained by FEM, RBF, and CN methods.

In Fig. 3 we report the estimated solution of $|E|$, E_{r}, E_{i}, and N at $t = 0$–10. We obtain this result with $h = 0.5$, $\Delta t = 10^{-1}$, and $d_{\mathrm{scale}} = 3$. We listed error norms of $|E|$, E_{r}, E_{i}, and N at $t = 10$ in Table 6. Compared with Table 5, it can be found that the error norms, when $t = 10$, increases rapidly. If the parameters used in Table 5 are consistent with those used in Table 4, the error norms should be smaller than those in Table 6. However, if we do that, it will take a lot of time and a large amount of calculation. In short, from the figures and tables, we can see that the numerical results obtained by the EFG method are in good agreement with the exact solution.

To illustrate the accuracy of our method, the model equation for the coupled Schrödinger-KdV equations can also be solved in the following form

$$\mathrm{i}E_t = E_{xx} + NE, \tag{55}$$

$$N_t + 6NN_x + N_{xxx} = (|E|^2)_x, \tag{56}$$

the initial and boundary conditions are the same as Eqs. (14) and (15). The soliton exact solutions are given[21] by

$$E(x,t) = \mathrm{e}^{\mathrm{i}\theta}[-\sqrt{2}(2c_2\pm\delta)+6\sqrt{2}c_2\,\mathrm{sech}^2(\sqrt{c_2}\xi)], \tag{57}$$

$$N(x,t) = -\frac{1}{3}(p+6c_2\pm\delta)+6c_2\,\mathrm{sech}^2(\sqrt{c_2}\xi), \tag{58}$$

where $\xi = x+2pt$, $\theta = px+(p+3p^2\pm\delta)t/3$, and $\delta = \sqrt{\sqrt{2}c_1c_3+4c_2^2}$. c_1, c_3, and $c_2 > 0$ are arbitrary constants. For simplicity, $c_1 = c_3 = 0$ are used.

In this example, the computation was carried out with parameters $\alpha = 10^{10}$, we take scaling parameter $d_{\mathrm{scale}} = 2.5$, time step length $\Delta t = 0.001$, spatial interval [–30, 30], and the spatial step size $h = 0.5$. In Fig. 4, the exact solutions of this problem are plotted in comparison with the numerical results

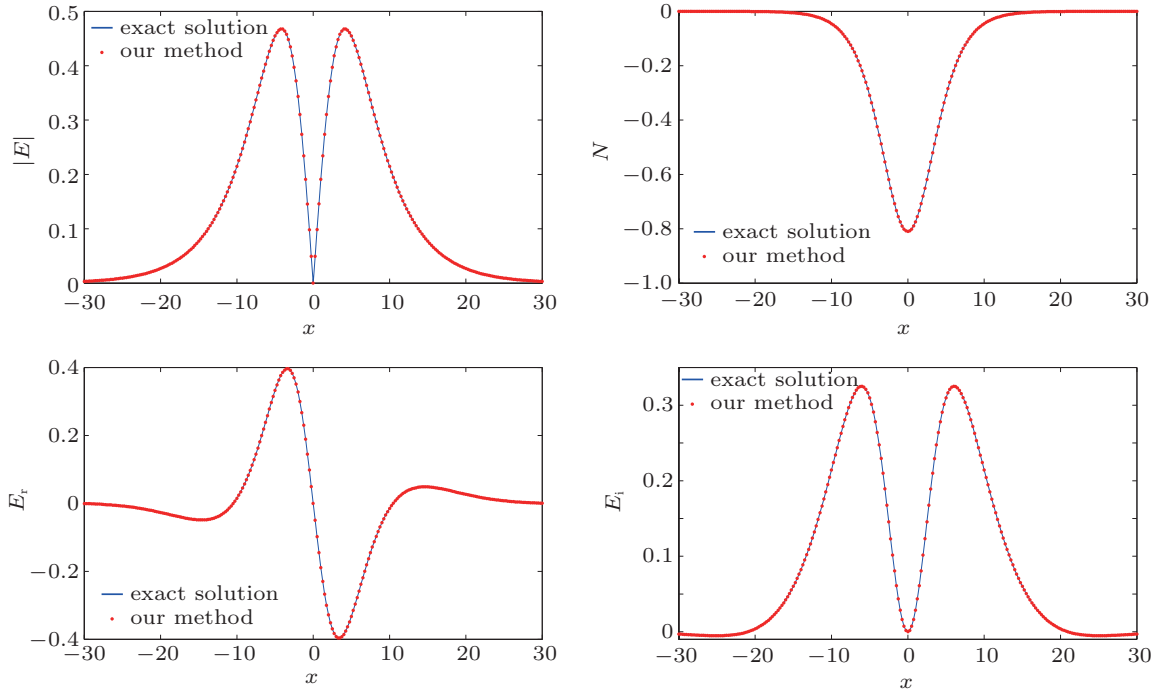


Fig. 1. (color online) Exact solution and estimated solution at $t = 0.001$ with $h = 0.25$ and $d_{\text{scale}} = 2.1$.

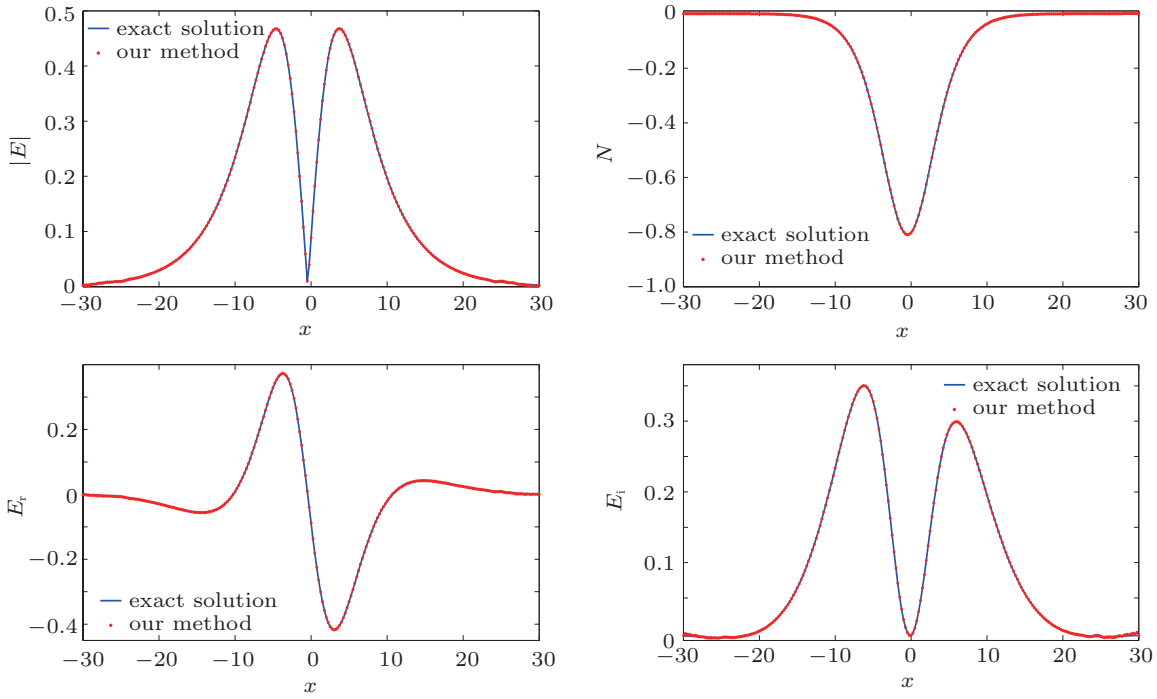


Fig. 2. (color online) Exact solution and estimated solution at $t = 1$ with $h = 0.25$ and $d_{\text{scale}} = 2.1$.

Table 1. Comparison of estimated solutions with the exact solution and other methods for the real part of E at $t = 0.001$ with $d_{\text{scale}} = 2.2$, $h = 0.25$.

x	CN	FEM	RBF	EFG	Exact solution
–20	-2.6616×10^{-2}	-2.6605×10^{-2}	-2.6597×10^{-2}	-2.6597×10^{-2}	-2.6597×10^{-2}
–10	1.5950×10^{-2}	1.5208×10^{-2}	1.5184×10^{-2}	1.5188×10^{-2}	1.5188×10^{-2}
0	5.2367×10^{-5}	1.4376×10^{-5}	-4.4634×10^{-5}	-8.9280×10^{-5}	-8.9284×10^{-5}
10	-1.5952×10^{-2}	-1.5172×10^{-2}	-1.5186×10^{-2}	-1.5200×10^{-2}	-1.5200×10^{-2}
20	2.6616×10^{-2}	2.6584×10^{-2}	2.6592×10^{-2}	2.6592×10^{-2}	2.6592×10^{-2}

Table 2. Comparison of estimated solutions with the exact solution and other methods for the imaginary part of E at $t = 0.001$ with $d_{\text{scale}} = 2.1$, $h = 0.25$.

x	CN	FEM	RBF	EFG	Exact solution
–20	3.8986×10^{-3}	3.7888×10^{-3}	3.7931×10^{-3}	3.7904×10^{-3}	3.7904×10^{-3}
–10	2.1445×10^{-1}	2.1441×10^{-1}	2.1427×10^{-1}	2.1428×10^{-1}	2.1428×10^{-1}
0	3.5376×10^{-3}	1.0657×10^{-5}	4.4932×10^{-5}	6.9733×10^{-8}	3.0133×10^{-9}
10	2.1425×10^{-1}	2.1425×10^{-1}	2.1425×10^{-1}	2.1424×10^{-1}	2.1424×10^{-1}
20	3.8986×10^{-3}	3.7931×10^{-3}	3.7926×10^{-3}	3.7915×10^{-3}	3.7915×10^{-3}

Table 3. Comparison of estimated solutions with the exact solution and other methods for N at $t = 0.001$ with d_{scale}=2.1, $h = 0.25$.

x	CN	FEM	RBF	EFG	Exact solution
–20	-6.7188×10^{-4}	-6.6905×10^{-4}	-6.6997×10^{-4}	-6.6886×10^{-4}	-6.6886×10^{-4}
–10	-4.5448×10^{-2}	-4.5268×10^{-2}	-4.5294×10^{-2}	-4.5256×10^{-2}	-4.5256×10^{-2}
0	-8.1000×10^{-1}	-8.1000×10^{-1}	-8.1000×10^{-1}	-8.1000×10^{-1}	-8.1000×10^{-1}
10	-4.5048×10^{-2}	-4.5228×10^{-2}	-4.5202×10^{-2}	-4.5239×10^{-2}	-4.5239×10^{-2}
20	-6.6560×10^{-4}	-6.6843×10^{-4}	-6.6747×10^{-4}	-6.6861×10^{-4}	-6.6861×10^{-4}

Table 4. Comparison of L_2 error norms for estimated solutions at $t = 0.001$ with $d_{\text{scale}} = 2.1$, $h = 0.25$.

	L_2 (CN)	L_2 (FEM)	L_2 (RBF)	L_2 (EFG)
E_{r}	3.4776×10^{-3}	2.5407×10^{-4}	1.6756×10^{-4}	1.2605×10^{-4}
E_{i}	2.0203×10^{-3}	3.6691×10^{-4}	1.6525×10^{-4}	8.701×10^{-6}
N	3.3631×10^{-4}	1.5194×10^{-5}	4.1078×10^{-4}	1.1237×10^{-7}

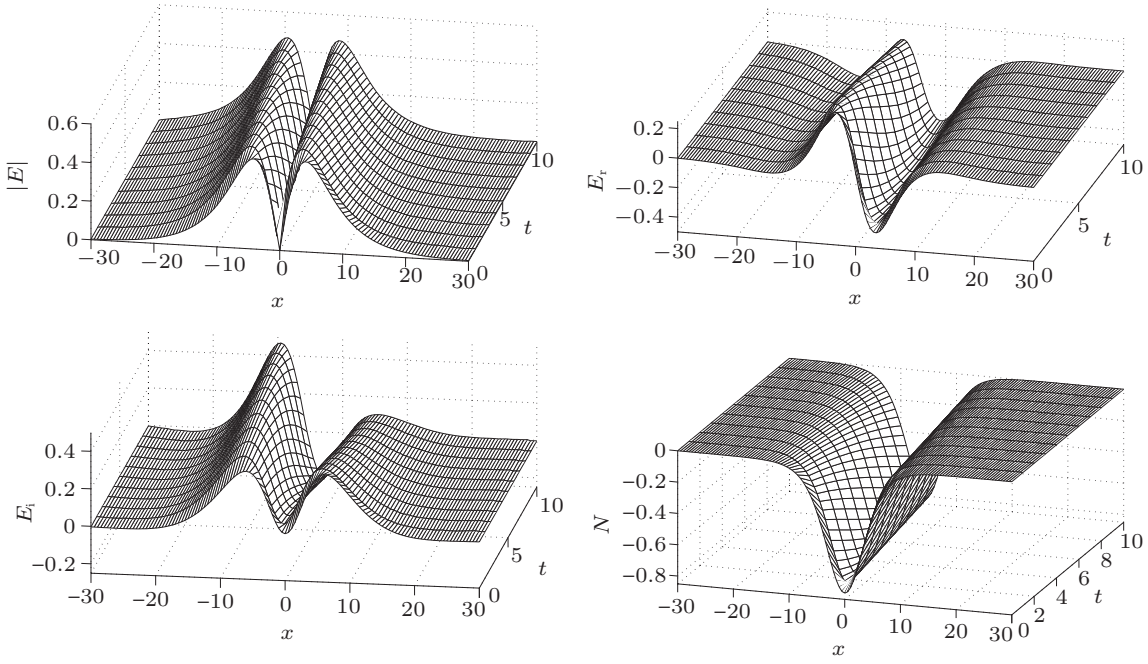


Fig. 3. Estimated solution at $t = 0$–10 with $h = 0.5$ and $d_{\text{scale}} = 3$.

Table 5. Comparison of L_∞ error norms for estimated solutions at $t = 0.001$ with $d_{\text{scale}} = 2.1$, $h = 0.25$.

	E_{r}	E_{i}	N
L_∞ (RBF)	7.7949×10^{-5}	7.3429×10^{-5}	1.2973×10^{-4}
L_∞ (EFG)	1.8523×10^{-4}	9.5779×10^{-6}	6.4861×10^{-8}

Table 6. Error norms for estimated solutions obtained by the EFG method at $t = 10$ with $d_{\text{scale}} = 3$, $h = 0.5$.

	E_{r}	E_{i}	N
L_2	9.2756×10^{-3}	1.4165×10^{-2}	2.0881×10^{-3}
L_∞	3.4798×10^{-3}	9.5305×10^{-3}	7.7429×10^{-4}

when $t = 1$, $c_2 = 0.01$, and $p = 0.1$. In Fig. 6, the exact solutions of this problem are plotted in comparison with the numerical results when $t = 1$, $c_2 = 0.01$, and $p = 1$. In Figs. 5 and 7 we show the estimated solution of $|E|$, E_{r}, E_{i}, and N at $t = 0$–1 with different parameters. Some results are also given in Table 7. A clear conclusion can be drawn from the results that the EFG method provides highly accurate solutions for the coupled Schrödinger-KdV equations.

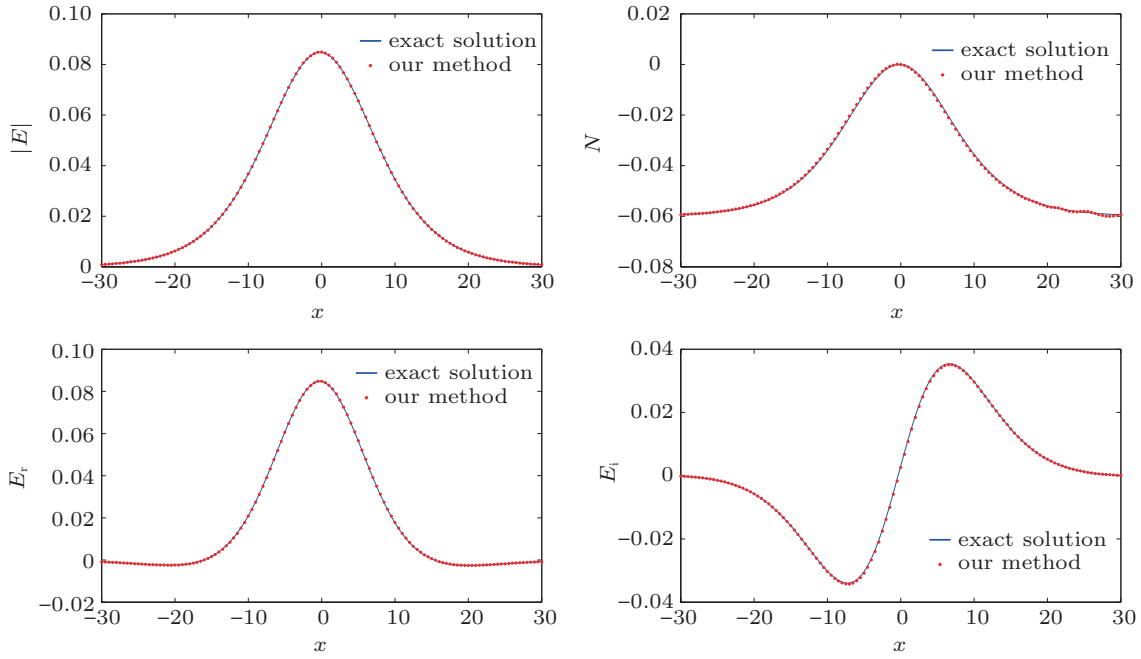


Fig. 4. (color online) Exact solution and estimated solution at $t = 1$ with $c_2 = 0.01$ and $p = 0.1$.

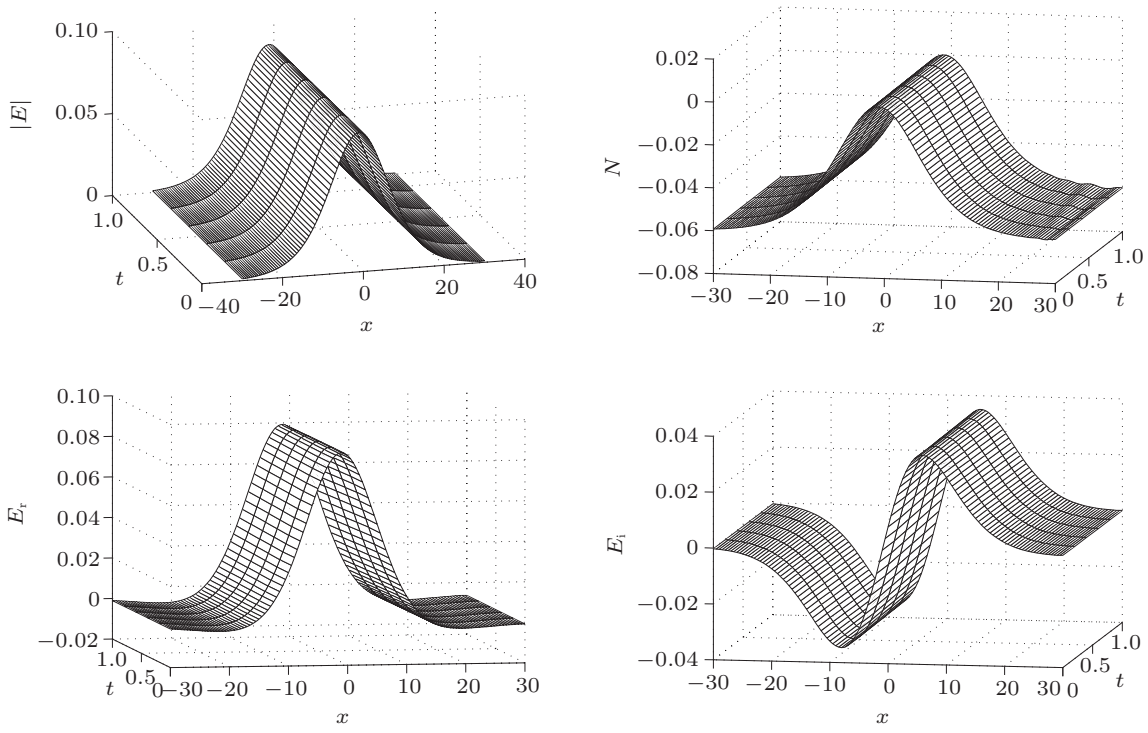


Fig. 5. Estimated solution at $t = 0$–1 with $c_2 = 0.01$ and $p = 0.1$.

Table 7. Error norms for estimated solutions obtained by the EFG method at $t = 1$ with different parameters.

		E_r	E_i	N
$p = 0.1$	L_2	1.3811×10^{-3}	2.558×10^{-3}	3.8042×10^{-3}
$c_2 = 0.01$	L_∞	2.3439×10^{-4}	5.6446×10^{-4}	8.7142×10^{-4}
$p = 1$	L_2	1.3751×10^{-3}	1.3751×10^{-3}	6.4793×10^{-3}
$c_2 = 0.01$	L_∞	3.6557×10^{-4}	3.704×10^{-4}	2.5088×10^{-3}

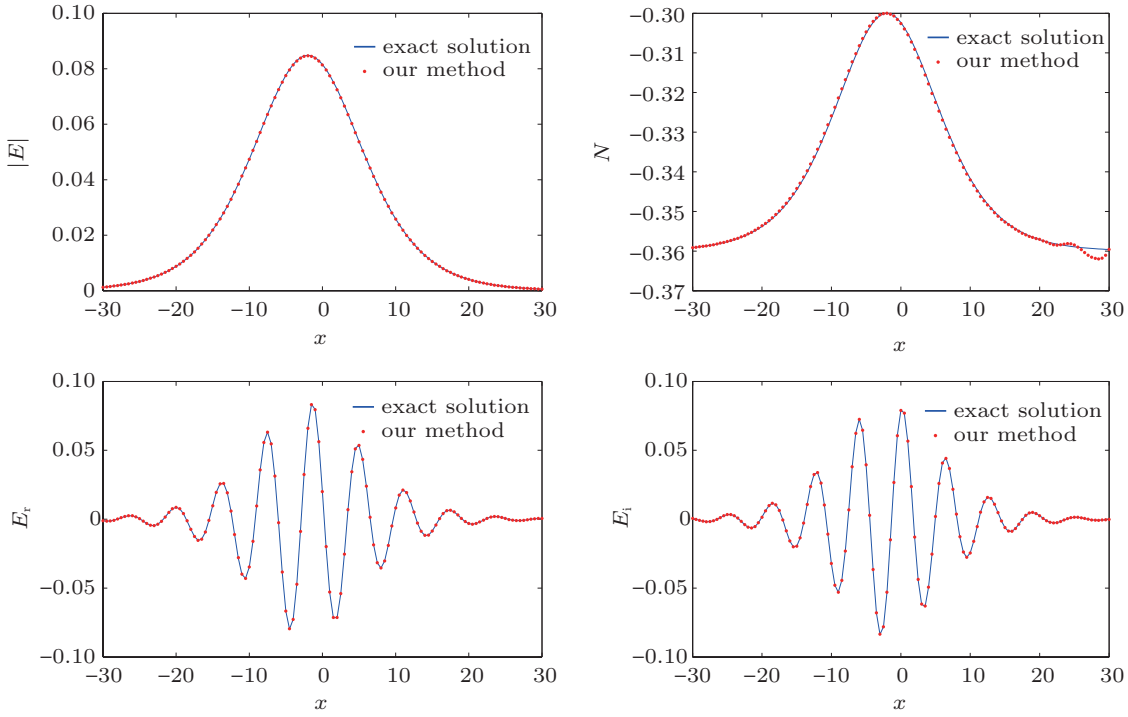


Fig. 6. (color online) Exact solution and estimated solution at $t = 1$ with $c_2 = 0.01$ and $p = 1$.

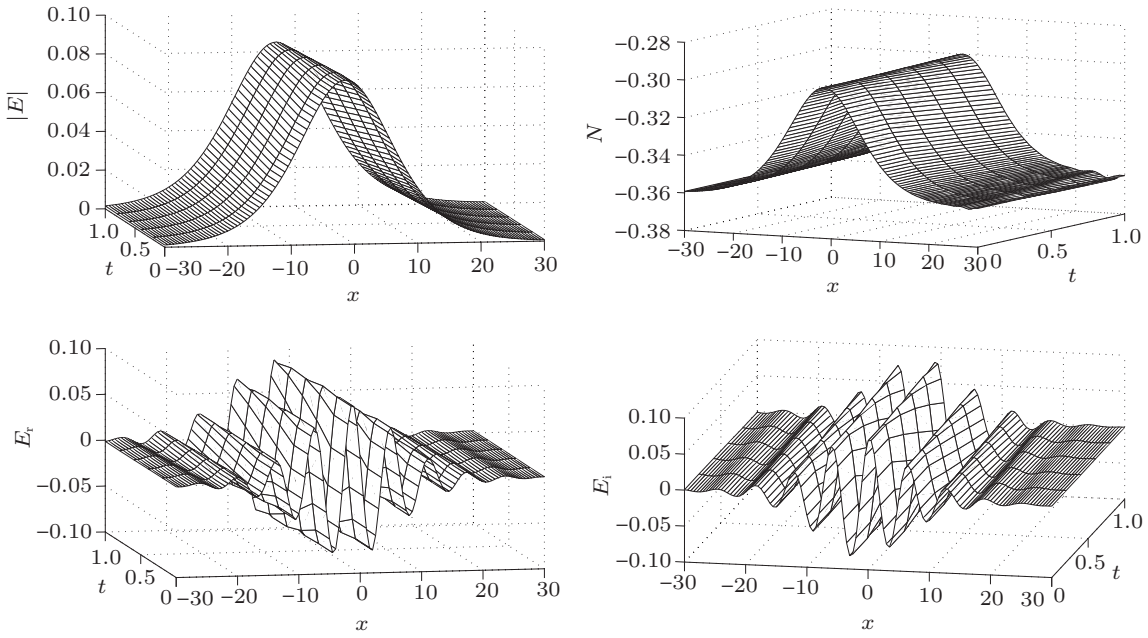


Fig. 7. Estimated solution at $t = 0$–1 with $c_2 = 0.01$ and $p = 0.1$.

5. Conclusions

In summary, we have applied the element-free Galerkin (EFG) method for the numerical solution of the coupled Schrödinger-KdV equations. The meshless property of the EFG method is the most important advantage of this scheme over the traditional mesh-dependent techniques such as the FEM and the FDM. The efficiency of the method is verified by making comparisons with the FEM, the RBF method, and the CN scheme. The numerical results are in good agreement with the analytical solutions. Moreover the numerical results, L_2 error norms are presented. The problem presented in this paper suggest that the mess-free approximation method should be considered as one of the possible ways for solving the coupled Schrödinger-KdV equations.

References

[1] Appert K and Vaclavik J 1977 *Phys. Fluids* **20** 1845

[2] Nishikawa K, Hojo H, Mima K and Ikezi H 1974 *Phys. Rev. Lett.* **33** 148
[3] Wang H 2005 *Appl. Math. Comput.* **170** 17
[4] Makhankov V G 1974 *Phys. Lett. A* **50** 42
[5] Bao W Z and Jaksch D 2003 *SIAM. J. Numer. Anal.* **41** 1406
[6] Kucakarslan S 2009 *Nonlinear Anal. Real Word Appl.* **10** 2264
[7] Bai D and Zhang L 2011 *Commun. Nonlinear Sci. Numer. Simul.* **16** 1263
[8] Pereira N R, Sudan R N and Denavit J 1977 *Phys. Fluids* **20** 271
[9] Abdou M A and Sdiman A A 2005 *Physica D* **211** 1
[10] Kaya D 2003 *Phys. Lett. A* **313** 82
[11] Bai D and zhang L 2009 *Phys. Lett. A* **373** 2237
[12] Golbabai A and Safdari-Vaighani A 2011 *Computing* **92** 225
[13] Wang J F, Sun F X and Cheng R J 2010 *Chin. Phys. B* **19** 060201
[14] Cheng R J and Ge H X 2009 *Chin. Phys. B* **18** 4059
[15] Cheng R J and Cheng Y M 2011 *Chin. Phys. B* **20** 070206
[16] Du C 2000 *Comput. Meth. Appl. Mesh. Engng.* **182** 89
[17] Kryl P and Belytschko T 1995 *Comput. Mech.* **17** 26
[18] Belytschko T, Krongauz Y, Organ D, *et al.* 1996 *Comput. Meth. Appl. Mech. Engn.* **139** 3
[19] Rubin S G and Graves R A 1975 Nasa TR R-436, Washington DC
[20] Guo B and Shen L 1982 *Proceedings of DD-3 Symposium*, Changchun, China, p. 417
[21] Fan E G 2002 *J. Phys. A: Math. Gen.* **35** 6853